Review of Scientific Instruments

Single-shot frequency-resolved optical gating for retrieving the pulse shape of high energy picosecond pulses

Cite as: Rev. Sci. Instrum. **89**, 103509 (2018); https://doi.org/10.1063/1.5044526
Submitted: 13 June 2018 . Accepted: 08 September 2018 . Published Online: 26 October 2018

R. Aboushelbaya, A. F. Savin, L. Ceurvorst, J. Sadler, P. A. Norreys, A. S. Davies, D. H. Froula, A. Boyle, M. Galimberti, P. Oliveira, B. Parry, Y. Katzir, and K. Glize

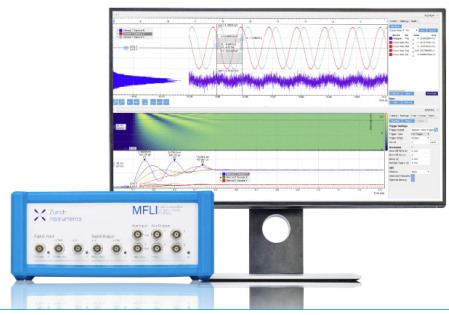

Single-shot frequency-resolved optical gating for retrieving the pulse shape of high energy picosecond pulses

R. Aboushelbaya,[1,a)] A. F. Savin,[1] L. Ceurvorst,[1] J. Sadler,[1] P. A. Norreys,[1,2] A. S. Davies,[3] D. H. Froula,[3] A. Boyle,[2] M. Galimberti,[2] P. Oliveira,[2] B. Parry,[2] Y. Katzir,[2] and K. Glize[2]
[1]*Clarendon Laboratory, Unversity of Oxford, Parks Road, Oxford OX1 3PU, United Kingdom*
[2]*Central Laser Facility, STFC Rutherford Appleton Laboratory, Didcot OX11 0QX, United Kingdom*
[3]*Physics Department and Laboratory for Laser Energetics, University of Rochester, Rochester, New York 14636, USA*

(Received 13 June 2018; accepted 8 September 2018; published online 26 October 2018)

Accurate characterization of laser pulses used in experiments is a crucial step to the analysis of their results. In this paper, a novel single-shot frequency-resolved optical gating (FROG) device is described, one that incorporates a dispersive element which allows it to fully characterize pulses up to 25 ps in duration with a 65 fs per pixel temporal resolution. A newly developed phase retrieval routine based on memetic algorithms is implemented and shown to circumvent the stagnation problem that often occurs with traditional FROG analysis programs when they encounter a local minimum. *Published by AIP Publishing.* https://doi.org/10.1063/1.5044526

I. INTRODUCTION

As laser pulses become an essential element of many experiments in various scientific fields ranging from quantum information to the physics of fusion, the precise measurement of these pulses becomes an increasingly important task. For sufficiently long pulses (>30 ps), high temporal resolution optical streak cameras used in conjunction with optical spectrometers are able to characterize the pulses spectrally and temporally. However, for short pulses, other methods must be used to measure the temporal evolution of the pulse; one notable example is frequency-resolved optical gating (FROG)—originally developed by Trebino.[1] However, with most current commercial single-shot FROG devices, the maximum pulse length that can be measured is limited to ~5 ps.[2]

To that end, a novel single-shot FROG device based on second-harmonic generation has been developed for the short pulse of the Vulcan laser at the Central Laser Facility.[3] This instrument can measure pulses up to a theoretical limit of 25 ps. High energy laser facilities are home to many important high energy density (HED) science experiments. Laser-plasma instabilities, such as stimulated Raman scattering (SRS), are heavily studied processes not only to gain a better understanding of the fundamental physics behind the interactions, but also for their applications in areas such as inertial confinement fusion,[4] laser-plasma particle accelerators,[5] and Raman amplification.[6] To be able to properly interpret the results of experiments conducted at these facilities,[3] accurate characterization of the laser pulses is required.

To be able to analyze the results from our second-harmonic generation FROG, we have also developed a retrieval algorithm based on memetic algorithms used in two-dimensional phase retrieval. Such algorithms are advantageous compared to the traditional iterative Fourier transform-based algorithms which tend to stagnate at times when they encounter a local minimum in the solution space, thus preventing them from converging to the optimal solution and properly retrieving the pulse.

In this paper, the design of the single-shot FROG diagnostic device is presented in Sec. II. In Sec. III, the new memetic algorithm is described, as are its advantages over the traditional iterative Fourier transform algorithms. In Sec. IV, some experimental results are presented for two distinctly different pulse measurements and the limitations of the device in range and resolution are discussed. Finally, a summary of the research and the potential future developments is presented in Sec. V.

II. DESIGN

A FROG device is usually composed of two main parts: an autocorrelator and a spectrometer. In traditional autocorrelators, the pulse is split using a 50/50 beam splitter and one half is propagated through a variable delay stage. A nonlinear-process combining the two halves of the split pulse (either second- or third-harmonic generation, for example) generates a signal, called an autocorrelation, that is a function of the delay between the pulses. By taking Fourier transform of the autocorrelation at different delays using the spectrometer, one generates a two-dimensional (2D) signal that is resolved in both frequency and time. This is the FROG trace. One disadvantage of these traditional systems is that to generate the full trace, multiple shots are needed to capture the signal at different delays and the temporal resolution is limited by the size of the steps of the variable delay stage.

Our design is based on second-harmonic generation, where the pulse halves are recombined on a barium borate (BBO) crystal to generate the autocorrelation. However, instead of using a variable delay stage, the pulses are recombined at an angle. As shown in Fig. 1, this causes different points on the crystal's axis to have different delays between the pulse halves. That way, the time delay axis of the

a)Electronic mail: ramy.aboushelbaya@physics.ox.ac.uk

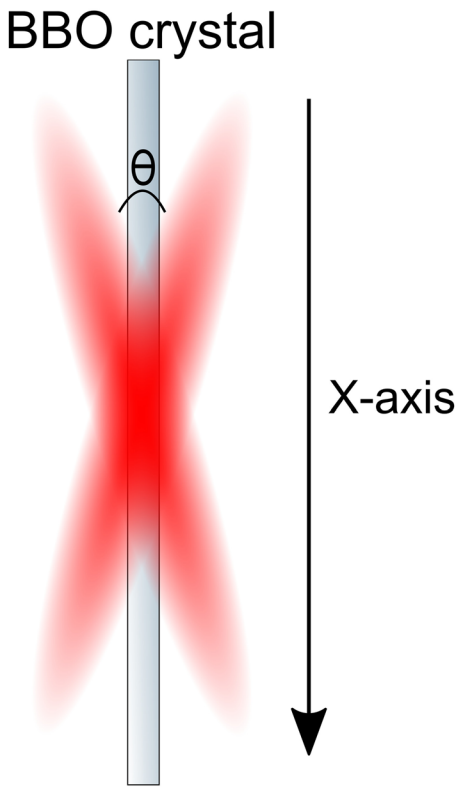

FIG. 1. Diagram showing the two pulses mixing at angle θ on the second-harmonic generation crystal. The bigger the angle, the larger the maximum temporal window of the autocorrelator.

autocorrelation is mapped onto the transverse spatial axis of the crystal, thus getting a full autocorrelation in a single shot. The temporal window of the FROG can be expressed as follows:[7]

$$\tau(x) = 2(x/c)\sin(\theta/2). \quad (1)$$

The maximum temporal window of the FROG can then be shown to be $\tau_{max} = (2d/c)\tan(\theta/2)$,[7] where d is the diameter of the beam and θ is the recombination angle between the two pulse halves, as shown in Fig. 1. This technique allows for a full FROG trace with each shot. Both the traditional scanning FROG devices and their single-shot counterparts have their advantages and disadvantages. The former is agnostic to the quality of the transverse profile of the beam and does not require the use of large imaging spectrometers. However, as the latter nets the full FROG trace in a single-shot, it is better suited for use with high power laser systems as they usually have a low repetition rate and can have a significant variation between shots which would make the use of the scanning FROG highly impractical. It also proves very useful for certain applications where only a limited number of laser shots are available such as in certain high intensity laser facilities.[3,8]

The single-shot FROG has been used extensively in many experiments across a varied number of scientific disciplines;[9–11] however, with most current commercially available single-shot FROG devices, their temporal window is limited to around ~5 ps.[2] In order to be able to measure longer pulses, a diffraction grating has been used to add a pulse-front tilt to the laser pulse. By doing so, the recombination angle increases, increasing the maximum temporal window up to a theoretical limit of 25 ps. It should be noted that there is a trade-off between the size of the temporal window and the temporal resolution of the device; this can be adjusted by changing the diffraction order used by the autocorrelator. With the zeroth order, there is no pulse-front tilt and so the temporal window is at its minimum and by using higher orders, the size of the window is increased.

Figure 2(a) shows a schematic of the FROG, clearly indicating that the autocorrelation is then split using a 50/50 beam splitter, where one half of the signal is imaged onto a charged coupled device (CCD). This camera helps with the alignment of the pulse in the autocorrelator so that second-harmonic generation can first be confirmed before aligning the rest of the device. The second half is then focused using a cylindrical lens onto the slit of a Princeton Instruments Spectra Pro SP300 spectrometer to measure Fourier transform of the autocorrelation along one axis. This is because for a single-shot measurement, one axis contains the spectral information and the other contains all the time delay information. Due to the design of the slit of this spectrometer, the second harmonic had to be inverted using a periscope in order to get the proper axis on the grating, as shown in Fig. 2(b).

The device was aligned using a high-repetition oscillator that produces short pulses that are only visible using an IR viewer. The challenge with aligning the second-harmonic into the spectrometer lies with the fact that it is very weak. To combat this, a green diode laser is fed into the device and aligned with the second-harmonic. This is accomplished by putting two irises and using the autocorrelation camera to ensure that the green laser and the second-harmonic are co-propagating.

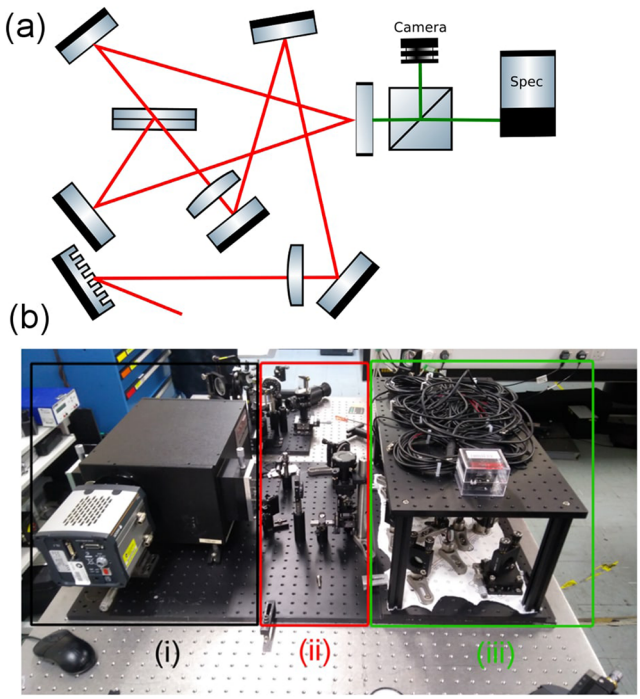

FIG. 2. (a) Schematic detailing the major optical components of the FROG. (b) (i) The second-harmonic generation autocorrelator used to generate the second harmonic signal for the FROG, (ii) the periscope and cylindrical lens used to flip the signal in the proper orientation and focus it onto the spectrometer's slit, and (iii) the PI SP-300 spectrometer with the Andor NEO camera used to generate the FROG signal.

Using this method, we have managed to transport the device between different locations on the site and align it successfully at these different locations using low-energy high repetition rate pulsed sources.

III. MEMETIC ALGORITHM

With the measured FROG trace, it is possible, using an appropriate retrieval algorithm, to determine the original pulse completely. This is despite the fact that the FROG trace contains only amplitude information about the spectrogram (spectrum of the autocorrelation) of the pulse. This process is referred to as two-dimensional phase retrieval. Unlike the one-dimensional case, it can be proven that there is a quasi-unique solution for each trace (except for a few trivial ambiguities such as the uncertainty in the absolute phase of the pulse[12]). In the case of the second-harmonic generation-FROG, there is an additional ambiguity as the direction of time cannot be determined due to the time reversal symmetry of the second-harmonic generation process.

Traditional FROG algorithms are usually based on an iterative Fourier transform/projection process that seeks to minimize an objective function which is measuring the error between a numerically simulated FROG trace (generated from an initial guess) and the experimentally measured trace. The most commonly used function for this is the mean-squared error which is defined at the i-th iteration to be as follows:[12]

$$F(E^{(i)}) = \sqrt{\frac{1}{N^2}\sum_{j,k=0}^{N} |I^{meas}_{FROG}(\tau_j,\omega_k) - I^{(i)}_{FROG}(\tau_j,\omega_k)|^2}, \quad (2)$$

where $I^{meas}_{FROG}(\tau_j,\omega_k)$ is the value of the measured FROG trace and $I^{(i)}_{FROG}(\tau_j,\omega_k)|$ is the value of the simulated FROG trace generated from the i-th iteration of the estimation of the pulse's electric field $E^{(i)}$. As these functions are discrete, the temporal and spectral axes are labeled by j and k, respectively.

This method is known to generally converge well if the objective function is convex over the space of possible solutions.[12] Unfortunately, this is often not the case for FROG measurements.

To illustrate this, the FROG trace of an unchirped double pulse, shown in Fig. 3(a), was numerically generated. Many guesses "close" to the true signal were then generated by varying two parameters: the duration of the double pulse and its chirp. The objective function was computed for all of these guesses. In general, the actual solution space has more than two dimensions, but we have restricted ourselves to these two parameters for purely illustrative reasons. The results are shown in Fig. 3(b).

It is clear from Fig. 3(b) that in addition to the global minimum at the correct parameters, there are multiple local minima at other parameter combinations. Within these minima, the traditional algorithm can stagnate and never reach the best possible estimation for the pulse. To combat this, a memetic algorithm that is based on a routine used in phase retrieval in x-ray diffraction[13] (a mathematically similar problem that faces many of the same obstacles) was used. Instead of starting with a single guess, this algorithm initializes many guesses simultaneously which means it explores multiple areas

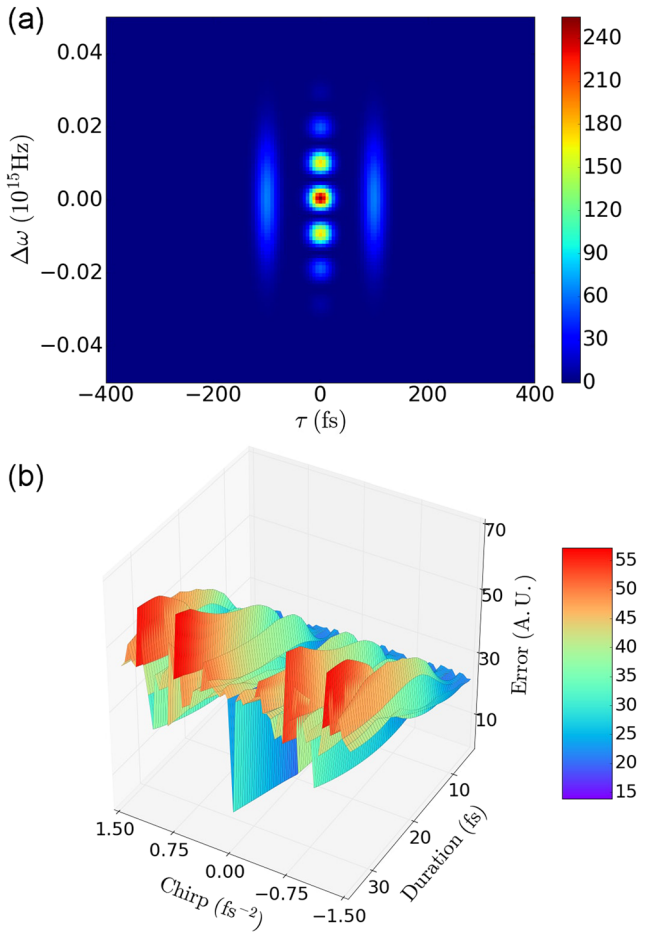

FIG. 3. (a) Numerical FROG trace produced from a double pulse showing the distinct interference pattern that is usually used to calibrate FROG devices and (b) 3D surface plot of the objective function across the two parameter scans of the guesses "around" the double pulse.

of the solution space at the same time. After performing a few iterations of the traditional iterative algorithm on each guess, it selects a sample of them quasi-randomly (with a bias for the "closest" guesses) and mixes them up to generate the population for the next iteration. There is also a probability of a random "mutation" happening that alters some components in the guesses. A beneficial consequence of these steps is that it is very difficult for the algorithm to get stuck in any local minimum.

This exploration can be quite slow especially when very large solution spaces are considered. However, combined with an efficient local improvement step that exploits each guess, the algorithm runs quite efficiently.[14] The flow chart in Fig. 4 gives the basic overview of one iteration of the retrieval routine which is expanded upon in Subsections III A–III G below.

A. Initialization

The first step in the algorithm is to generate an initial population of guesses. To do so, we start with some initial guess for the pulse, $E_{init}(t)$. The initial population $\{E_i(t)\}_{i=1,\ldots,N}$ is then generated by randomly changing the phase at each time step of each pulse,

$$E_i(t_j) = |E_{init}(t_j)| \exp(i\phi_j),$$
$$\phi_j = \arg(E_{init}(t_j)) + R \cdot \mathrm{rand}[-\pi,\pi]. \quad (3)$$

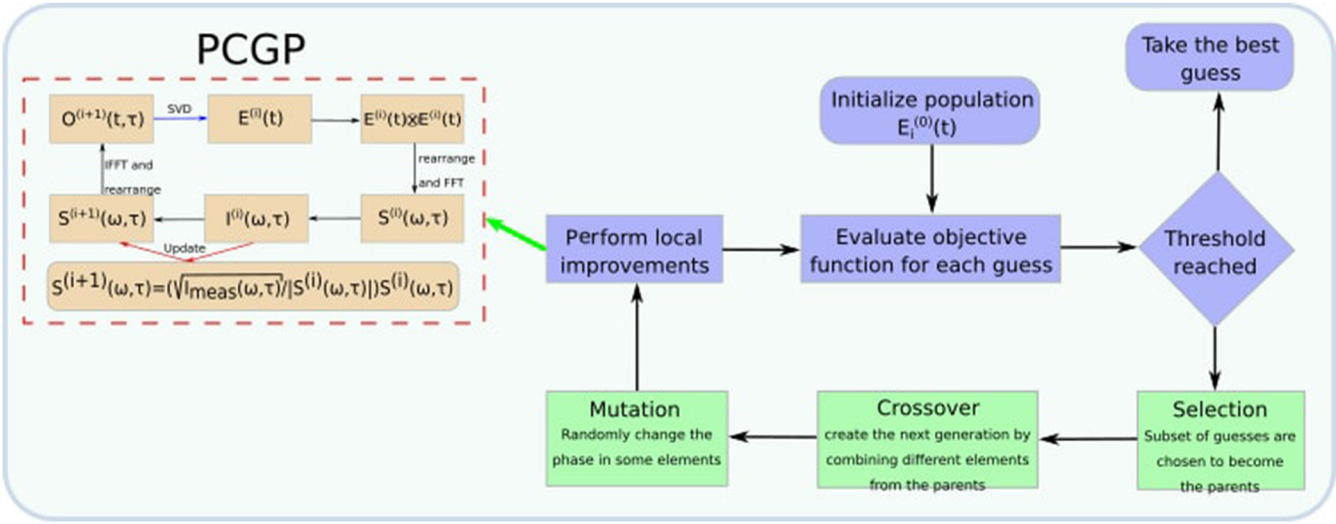

FIG. 4. Flow chart of the memetic algorithm.

The parameters that govern this step are $N \in \mathbb{N}$, the size of the population used in the algorithm, and $R \in [0, 1]$, the degree of randomness in generating the initial population out of the initial guess. N can greatly affect the performance of the algorithm; by increasing it, there are more guesses that explore the solution space; however, this is at the cost of considerably slowing down the algorithm as there are many elements that have to go through the local improvement.

B. Selection

This is a crucial step in the algorithm as it is the process by which elements of the population are chosen to become "parents" for the next generation. First, the current population is ordered with respect to the objective function (in our case the mean squared error) from best to worst. The algorithm then draws from a biased distribution to get the ranking of the element that will be selected. A bias that heavily favors the best elements will speed up the convergence. However, it runs the risk of getting stuck in a local minimum as it does not explore the solution space. On the other hand, choosing elements completely randomly, while it increases the exploration, runs the risk of taking too much computing time. The ranking is drawn using the following distribution:

$$n = \left\lfloor (\mathrm{rand}(0, 1)^{\beta}) \cdot N \right\rfloor + 1. \tag{4}$$

The parameter that controls this step is $\beta \geq 1$, which adjusts the bias of the distribution.

C. Crossover

In this step, the next generation of guesses is produced. Inspired by the genetic crossover that is the driver of natural evolution,[15] differential crossover randomly mixes different components from the parents. Using the selection process outlined above, four parents are chosen. The offspring are then created as follows:

$$E_{new}(t_j) = \begin{cases} E_1(t_j) & \text{if rand}[0, 1) \geq C, \\ E_2(t_j) + D \cdot (E_3(t_j) - E_4(t_j)) & \text{else,} \end{cases} \tag{5}$$

where $C \in [0, 1]$, called the balancing coefficient, controls how much crossover happens at each iteration and D, called the differential coefficient, controls the contribution of the third and fourth parents.

The number of offspring can in fact be smaller than the current population size, $N_o = G{\cdot}N$, where $G \in [0, 1]$ is usually called the genetic function.[13] In those cases, the next generation is supplemented with elements from the current one, also chosen using the biased distribution outlined in Sec. III B, so that all the generations have the same size as the initial one.

D. Mutation

In this step, for each element, the phase of each time step is modified by adding a random phase,

$$E_i(t_j) = \begin{cases} E_i(t_j) & \text{if rand}[0, 1) \leq M, \\ E_i(t_j) \exp(\mathrm{i}R_M \cdot \mathrm{rand}[-\pi, \pi]) & \text{else,} \end{cases} \tag{6}$$

where $M \in [0, 1]$ is the mutation coefficient, which controls the likelihood of a mutation occurring at any given time step. $R_M \in [0, 1]$ controls the range of the added phase, hence controlling the "degree" of the mutation. This step increases the exploration of the solution space to regions that might not have been reached in the initialization step.

E. Local improvement

The last step in the cycle is subjecting each element of the current generation to several iterations of a traditional retrieval algorithm. In our case, the iterative Principal Component Generalized Projections (PCGP) algorithm, which is well suited for the second-harmonic generation FROG,[16] was used. For each guess vector $\mathbf{E}$, an autocorrelation matrix is created by computing the outer product $\mathbf{E}\mathbf{E}_{\mathrm{T}}$. By rearranging the matrix and taking the squared magnitude of its Fourier transform, a numerical FROG trace can be created, which then can be compared to the measured one. If the guess is not "close" enough, the magnitude of the rearranged matrix is replaced with the square root of the measured FROG. By performing a singular value decomposition (SVD) on the resulting matrix, it can

then be written as a product of two orthogonal matrices and a diagonal matrix. By taking the columns corresponding to the largest singular value in the diagonal matrix, the "improved" guess is attained. This process can, however, be computationally costly as larger matrices are used; however, it can be sped up by implementing what is called the power method.[16]

The parameter that controls this step is N_i which determines the number of iterations of the PCGP algorithm we run on each generation. At the end of the iteration, the objective function is again computed for all the members of the current population and the "best" guess is kept in memory as the routine goes into the next iteration.

F. Practical difficulties

A number of difficulties usually arise with this algorithm. The first is the choice of the parameters. Due to the large number of parameters that significantly impact the result of the algorithm, trial and error must be employed to determine the optimum set of parameters for each class of "similar" pulses. Also, as with most FROG retrieval algorithms, since there is an iterative Fourier transform step, the size of the temporal window and the frequency resolution are intrinsically related, as are the extent of the frequency window and the time resolution. More explicitly, if a large temporal window is required, the frequency resolution must be small enough to enable its calculation and vice versa, or else performing numerical Fourier transform would be impossible.

G. Comparing the memetic algorithm to traditional algorithms

To compare the performance of the memetic algorithm relative to just the traditional PCGP algorithm, both of them were used on the FROG trace generated by the double pulse used above to showcase the solution space in Fig. 3(a). The parameters used for the memetic algorithm were $N = 40$, $N_i = 10$, $R = 0.5$, $M = 1$, $C = 0.5$, $D = 0$, $G = 1$, and $\beta = 0.15$.

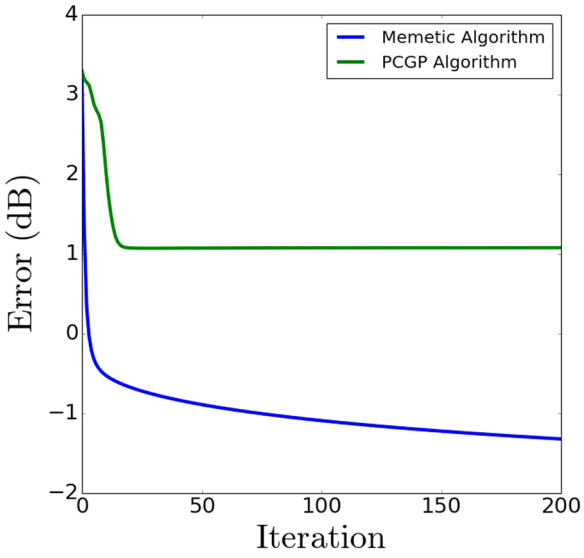

FIG. 5. The graph shows the different progression for the two algorithms. It should be noted that each iteration of the memetic algorithm contains multiple iterations of the local improvement using the PCGP.

As can clearly be seen in Fig. 5, the traditional algorithm encounters a local minimum and is unable to improve beyond it, no matter how many iterations are performed. However, the memetic algorithm does not get stuck and is able to continue and reduce the error by more than two orders of magnitude over ~100 iterations.

It should be noted that the memetic algorithm runs in ~30 min on a laptop. The main parameters that affect its runtime are N, N_i, the number of iterations of the full algorithm, and the size of the FROG trace, the latter of which would affect it if the power method is not used.

IV. EXPERIMENTAL RESULTS

The device was tested in two very different conditions. The first is measuring the output of a femtosecond oscillator which produces a train of pulses at a 50 Hz repetition rate with a pulse duration on the order of hundreds of femtoseconds. This is the source that was used to first calibrate the FROG. The calibration was done by introducing a prepulser between the oscillator and the device. The prepulser splits each pulse into two with equal energies, separated in time by a controllable delay. When two pulses enter the FROG, the trace has a very distinct shape, similar to the one shown in Fig. 3(a), which has three separate 2D peaks separated in time by the delay between the two pulses.[17] The central peak also shows a distinct spectral interference pattern where the peaks are separated with the reciprocal of the delay. By varying the delay and measuring the effect on the FROG traces, we can calibrate the spectral and temporal axis of the FROG trace. We find that the device has a pixel temporal resolution of 65 fs and a pixel spectral resolution of 0.01 nm.

After calibration of the device, the FROG trace produced by the oscillator, without the prepulser, is then run through the memetic retrieval algorithm. Figure 6(b) shows the results of this process. The retrieved pulse fits well with a Gaussian with a FWHM of 390.01 fs. The phase shows a slight chirp. The direction of this chirp is ambiguous since, as noted in Sec. III, both positive and negative chirps have the same effect on the trace of second-harmonic generation-FROG. There is, however, a way to break this symmetry by introducing a small prepulse.[17] This breaks the time reversal symmetry of the pulse which lifts the ambiguity in the retrieved pulse.

The device was then used to measure the pulse duration and relative phase shift of a high power short pulse from the Vulcan laser system.[3] Figure 7 shows the results of a measurement of the 10 J short pulse. It should be noted that the beam profile was smoothed using a random phase plate[18] both for the purposes of the experiment and because the single-shot FROG is quite sensitive to spatial non-uniformity. The FWHM of the retrieved intensity is 4.7 ps which is in the expected range, with the phase showing an ambiguous chirp. We have also confirmed this measurement by taking the spectrum of the retrieved pulse and comparing it to the independently measured spectrum of the laser. It should be noted that in all cases, the phase points of the retrieved signal that are beyond the temporal width of the intensity envelope were dropped as they convey no physical meaning since they represent points where the actual measured signal was below the intensity

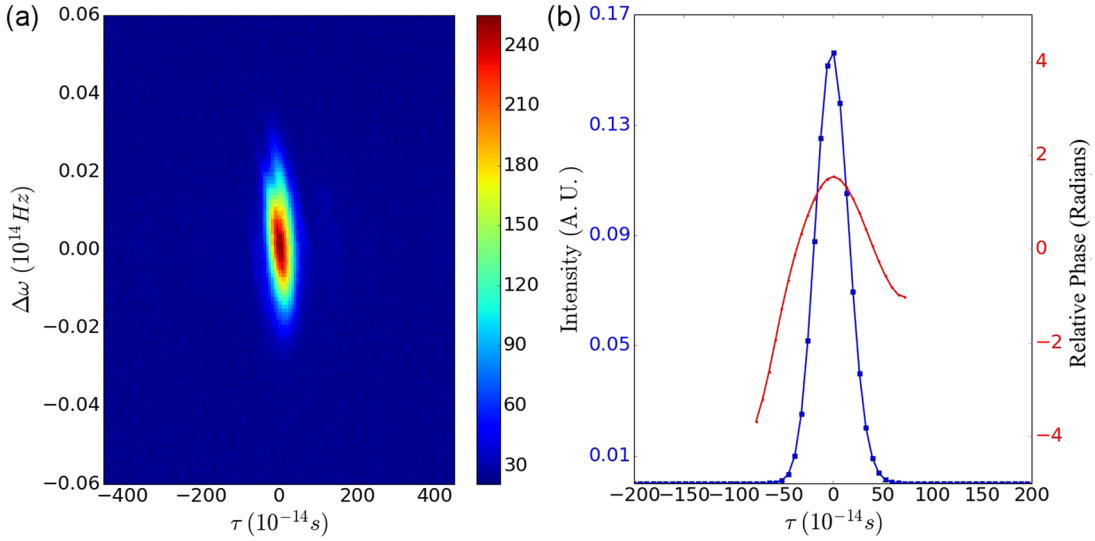

FIG. 6. (a) FROG trace produced by the femtosecond oscillator and (b) intensity of the retrieved pulse and its phase.

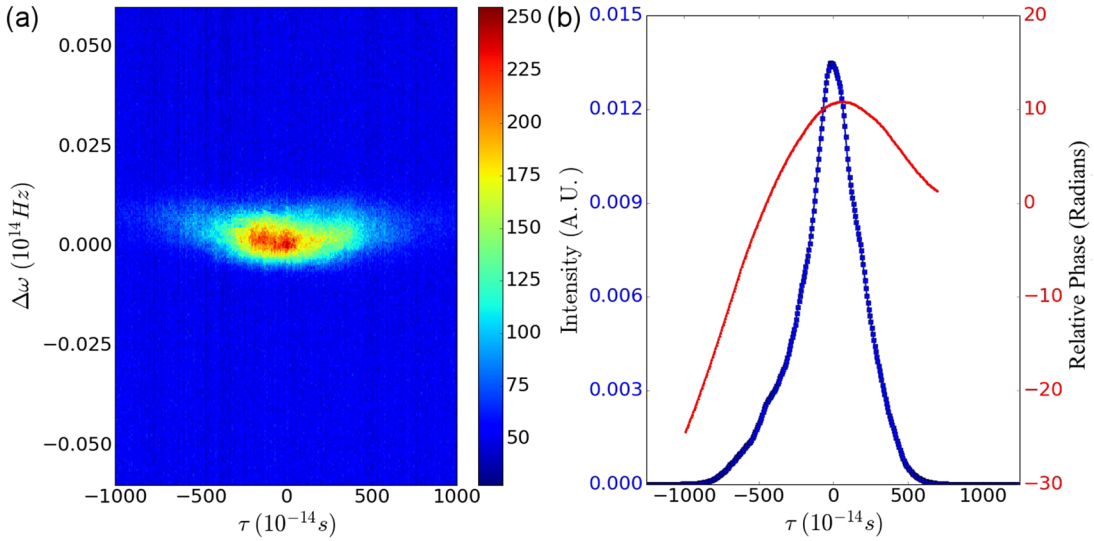

FIG. 7. (a) FROG trace produced by the Vulcan short pulse beam and (b) intensity of the retrieved pulse and its phase.

threshold required to register as a constituent part of the laser pulse.

V. CONCLUSION

A new single-shot FROG device based on second-harmonic generation was developed, one that can measure the duration and relative phase of high intensity pulses up to ~25 ps with high temporal resolution. This was achievable primarily due to the use of dispersive optical elements to introduce a pulse front tilt to a laser pulse so as to increase the maximal measurable temporal window. This is very relevant to characterize picosecond laser pulses used in many different high energy density physics experiments. The device was developed and tested on the Vulcan laser at the Central Laser Facility, Rutherford Appleton Laboratory. The new, relatively low-cost instrument is suitable for implementation on any short-pulse laser facilities, such as the OMEGA laser[19] and the National Ignition Facility.[8]

A novel memetic-style algorithm was developed for the retrieval of the pulses from the FROG trace. This algorithm avoids the stagnation problem that can happen with the traditional algorithm when it encounters a local minimum. By randomly exploring the solution space, the evolutionary algorithm seems to be resilient to the stagnation problem and continues to improve the guess beyond the traditional algorithm.

ACKNOWLEDGMENTS

This work has been carried out within the framework of the EUROfusion Consortium and has received funding from the Euratom research and training programme 2014-2018 under Grant Agreement No. 633053. This work has also been funded by EPSRC Grant No. EP/L000237/1, the Rutherford International Fellowship Programme, and the U.S. Department of Energy Office of Fusion Energy Sciences under Contract No. DE-SC0016253. The authors would also like to thank the staff

of the Central Laser Facility at the STFC Rutherford Appleton Laboratory.

[1]R. Trebino and D. J. Kane, J. Opt. Soc. Am. A **10**, 1101 (1993).
[2]D. Lee, S. Akturk, P. Gabolde, and R. Trebino, Opt. Express **15**, 760 (2007).
[3]C. N. Danson, P. A. Brummitt, R. J. Clarke, J. L. Collier, B. Fell, A. J. Frackiewicz, S. Hancock, S. Hawkes, C. Hernandez-Gomez, P. Holligan, M. H. R. Hutchinson, A. Kidd, W. J. Lester, I. O. Musgrave, D. Neely, D. R. Neville, P. A. Norreys, D. A. Pepler, C. J. Reason, W. Shaikh, T. B. Winstone, R. W. W. Wyatt, and B. E. Wyborn, Nucl. Fusion **44**, S239 (2004).
[4]P. Michel, L. Divol, E. Dewald, J. Milovich, M. Hohenberger, O. Jones, L. B. Hopkins, R. Berger, W. Kruer, and J. Moody, Phys. Rev. Lett. **115**, 055003 (2015).
[5]A. Modena, Z. Najmudin, A. E. Dangor, C. E. Clayton, K. A. Marsh, C. Joshi, V. Malka, C. B. Darrow, C. Danson, D. Neely, and F. N. Walsh, Nature **377**, 606 (1995).
[6]J. D. Sadler, R. M. Trines, M. Tabak, D. Haberberger, D. H. Froula, A. S. Davies, S. Bucht, L. O. Silva, E. P. Alves, F. Fiza, L. Ceurvorst, N. Ratan, M. F. Kasim, R. Bingham, and P. A. Norreys, Phys. Rev. E **95**, 053211 (2017).
[7]R. Trebino, *Frequency-Resolved Optical Gating: The Measurement of Ultrashort Laser Pulses* (Springer, Boston, MA, 2000), pp. 141–156.
[8]C. W. Siders, J. K. Crane, M. C. Rushford, L. C. Haefner, J. E. Hernandez, J. W. Dawson, R. J. Beach, W. J. Clark, D. J. Trummer, G. L. Tietbohl, and C. J. Barty, *10-kJ Status and 100-kJ Future for NIF Petawatt Technology* (2007), available at https://digital.library.unt.edu/ark:/67531/metadc895083/.
[9]S. Palaniyappan, R. C. Shah, R. Johnson, T. Shimada, D. C. Gautier, S. Letzring, D. Jung, R. Hrlein, D. T. Offermann, J. C. Fernndez, and B. M. Hegelich, Rev. Sci. Instrum. **81**, 10E103 (2010).
[10]S. Palaniyappan, B. M. Hegelich, H.-C. Wu, D. Jung, D. C. Gautier, L. Yin, B. J. Albright, R. P. Johnson, T. Shimada, S. Letzring, D. T. Offermann, J. Ren, C. Huang, R. Hörlein, B. Dromey, J. C. Fernandez, and R. C. Shah, Nat. Phys. **8**, 763 (2012).
[11]W. Theobald, R. Häßner, R. Kingham, T. Feurer, H. Schillinger, G. Schäfer, and R. Sauerbrey, *Ultrafast Phenomena XI* (Springer, Berlin Heidelberg, 1998), pp. 410–414.
[12]M. A. Krumbuegel and R. Trebino, *Frequency-Resolved Optical Gating: The Measurement of Ultrashort Laser Pulses* (Springer US, Boston, MA, 2000), pp. 157–178.
[13]A. Colombo, D. E. Galli, L. De Caro, F. Scattarella, and E. Carlino, Sci. Rep. **7**, 42236 (2017).
[14]T. El-Mihoub, A. A. Hopgood, L. Nolle, and A. Battersby, Eng. Lett. **13**, 124–137 (2006).
[15]H. B. Creighton and B. McClintock, Proc. Natl. Acad. Sci. U. S. A. **17**, 492 (1931).
[16]D. J. Kane, *Frequency-Resolved Optical Gating: The Measurement of Ultrashort Laser Pulses* (Springer, Boston, MA, 2000), pp. 357–366.
[17]E. Zeek, A. P. Shreenath, P. OShea, M. Kimmel, and R. Trebino, Appl. Phys. B **74**, s265 (2002).
[18]S. N. Dixit, I. M. Thomas, B. W. Woods, A. J. Morgan, M. A. Henesian, P. J. Wegner, and H. T. Powell, Appl. Opt. **32**, 2543 (1993).
[19]T. R. Boehly, R. S. Craxton, T. H. Hinterman, J. H. Kelly, T. J. Kessler, S. A. Kumpan, S. A. Letzring, R. L. McCrory, S. F. B. Morse, W. Seka, S. Skupsky, J. M. Soures, and C. P. Verdon, Rev. Sci. Instrum. **66**, 508 (1995).